International Journal of Solids and Structures 47 (2010) 3131–3140

Contents lists available at ScienceDirect

International Journal of Solids and Structures

journal homepage: www.elsevier.com/locate/ijsolstr

Analysis of the stress singularity field at a vertex in 3D-bonded structures having a slanted side surface

Hideo Koguchi [a,*], Joviano Antonio da Costa [b]

[a] Department of Mechanical Engineering, Nagaoka University of Technology, Kamitomioka 1603-1, Nagaoka, Niigata 940-2188, Japan
[b] Department of Mechanical Engineering, Graduate School of Nagaoka University of Technology, Kamitomioka 1603-1, Nagaoka, Niigata 940-2188, Japan

ARTICLE INFO

Article history:
Received 26 December 2009
Received in revised form 9 July 2010
Available online 3 August 2010

Keywords:
3D joints
Stress singularity
Intensity of singularity
Eigenanalysis
BEM

ABSTRACT

The stress singularity that occurs at a vertex in a joint with a slanted side surface is investigated. The orders of stress singularity at a vertex and at a point on stress singularity lines for various material properties are determined using eigenanalysis. The stress distribution on an interface and the intensity of stress singularity at the vertex are investigated using BEM. It is shown that the order of stress singularity at the vertex in the joints can be reduced by slanting a side surface so as to decrease the angle between the interface and the side surface. The results of BEM analysis reveal that the distribution of stress on the interface is influenced by the slanted side surface. Finally, the 3D intensities of the singularity for stress components which are continuous at the interface are newly defined and determined for various material combinations.

1. Introduction

In recent years, bonded dissimilar materials and composite materials have been widely used in many industrial products. With the increasing use of such materials, the demand for strength evaluation has also increased. Electronic device packagings have several types of joint structures consisting of metal, ceramic, and polymer. When two materials are joined, a free-edge stress singularity usually develops at the intersection of the interface and the free surface. Previous studies (Bogy, 1971; Inoue et al., 1995; Yang and Munz, 1995) have revealed that stress singularities occur near the cross point of the free surface and the interface, thereby reducing the reliability of the joints. Therefore, several theoretical and experimental studies on the reduction of the stress singularity have been carried out (Koguchi et al., 1994). Most of these studies focused on two-dimensional stress singularities (Bogy, 1971; Bogy and Wang, 1971; Hein and Erdogan, 1971; Cook and Erdogan, 1972; Theocaris, 1974; Fenner, 1976; Dempsey and Sinclair, 1979).

Several studies have investigated the stress singularity field in 3D elastic materials. Yamada and Okumura (1981) developed a finite element analysis for solving an eigenvalue equation to determine directly the order of stress singularity and the angular variation of the stress and displacement fields. Then, Pageau et al. (1995) adapted the eigenanalysis based on a finite element to analyze the in-plane deformation of wedges and junctions of anisotropic materials. The stress and displacement fields were obtained from eigenformulation for real and complex orders of stress singularity. Pageau and Biggers (1995), Pageau et al. (1996) applied this method to analyze joints having fully bonded multi-material junctions intersecting a free edge, and they determined the order of stress singularity and the angular variation of the displacement and stress fields around singular points in a plane intersecting a wedge front in 3D anisotropic material structures. Koguchi (1996), Koguchi and Muramoto (2000), Prukvilailert and Koguchi (2005) examined the order of stress singularity not only at a vertex but also along the stress singularity line between two isotropic materials in joints using eigenanalysis. The stress distributions around the vertex were determined using a boundary element method (BEM). Koguchi (2006) determined the intensity of singularity by fitting the stress profile obtained from BEM analysis with a least squares method. Dimitrov et al. (2001, 2002) presented a 3D eigenanalysis using the Arnoldi method, which, unlike the conventional determinant method, requires only a small-banded matrix. Constabel et al. (2001) proposed a method to compute their singularity exponents and the associated angular singular functions. Their method was particularly useful with anisotropic materials and allowed to follow the dependency of singularity exponents along a curved edge. Lee and Im (2003) used a two-state *M*-integral to compute the near-tip stress intensities around 3D wedges and used an eigenanalysis to determine eigenvalues and eigenvectors. Apel et al. (2008) determined the edge singularity using a 3D Williams' expansion. The edge stress intensity factors along the reentrant wedge front were determined using a quasi-dual function method. Yosibash et al. (2008) and Omer and Yosibash (2008) computed the complex eigenfunction using a *p*-version finite element

* Corresponding author. Fax: +81 258 47 9770.
E-mail address: koguchi@mech.nagaokaut.ac.jp (H. Koguchi).

0020-7683/$ - see front matter © 2010 Elsevier Ltd. All rights reserved.
doi:10.1016/j.ijsolstr.2010.07.015

method and examined the edge stress intensity factors in the vicinity of the edge in 3D anisotropic multi-material interfaces using a quasi-dual function method.

In the present paper, the influence of the variation of the angle between a side surface and an interface on the singular stress field at a vertex in 3D joints as shown in Fig. 1 is investigated. From previous studies, the singular stress field at the vertex O in Fig. 1 can be generally expressed as $\sigma_{ij}(r,\theta,\phi) = K_{1ij} f_{1ij}(\theta,\phi)\ r^{-\lambda} + K_{2ij}\ f_{2ij}(\theta,\phi)$, where K_{1ij} is intensity of singularity, $f_{1ij}(\theta,\phi)$ is an angular function for stress σ_{ij}, and r is a distance from the vertex. Here, θ and ϕ are angular coordinates in spherical coordinate system with an origin at the vertex as shown in Fig. 1. Intensity of the singularity at the vertex is newly defined including the influence of stress singularity lines on the side surfaces. The intensity of the singularity for a silicon-resin joint is first determined using the results of eigenanalysis and BEM, and the intensity of the singularity for joints of various material combinations is next determined. A relationship between the intensity of the singularity and a ratio of Young's modulus in joints of various material combinations for several different slant angle α will be demonstrated.

2. Method and model for analysis

2.1. Method for analysis

An eigenequation based on the finite element method (FEM) developed by Pageau et al. (1996) was used to analyze a singular stress state at the singular point in a 3D dissimilar material joint. In the formulation of the FEM, a spherical coordinate system with the origin at a stress singular point is introduced, and displacements within a sphere of radius r_0 in the stress singular field are expressed using the characteristic root p, which is related to the order of stress singularity. The surface of the sphere is divided by a mesh, and the FEM formulation for the stored energy in the sphere is derived. In the formulation, a stress free condition is applied. Finally, the following eigenequation is deduced, and the order of stress singularity is determined:

$$\left(p^2[\mathbf{A}] + p[\mathbf{B}] + [\mathbf{C}]\right)\{\mathbf{u}\} = 0, \tag{1}$$

where p represents the characteristic root, which is related to the order of singularity, λ, as $\lambda = 1 - p$, [**A**], [**B**], and [**C**] are matrices related to the material properties, and {**u**} represents the displacement vector.

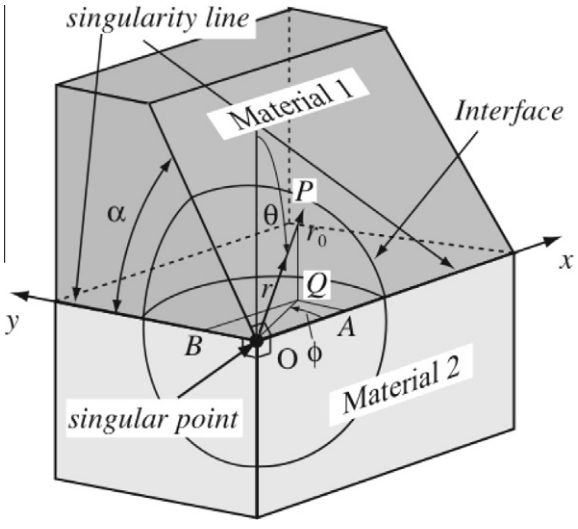

Fig. 1. Model for eigenanalysis.

The angular functions of the stress components are determined using the displacements vector {**u**}.

The boundary integral equation in terms of displacement vector u_j and traction vector t_j can be expressed as follows:

$$C_{ij}u_j(P) = \int_A \{U_{ij}(P,Q)t_j(Q) - T_{ij}(P,Q)u_j(Q)\}ds(Q), \tag{2}$$

where P and Q are points on the boundary, C_{ij} is a constant determined from the configuration of the boundary, and U_{ij} and T_{ij} are the fundamental solutions for displacement and surface traction, respectively. In the present analysis, Rongved's fundamental solution for two-phase isotropic materials was used. Hence, mesh on the interface is not needed for analysis, and so accurate stress distributions on the interface can be obtained.

2.2. Model for analysis

2.2.1. Model for eigenanalysis

The model used in the eigenanalysis is shown in Fig. 1. The model is of a 3D joint with a slanted side surface in material 1. Eigenanalysis is conducted for points as follows:

1. A point is located at the vertex. The slant angles of the side surface are 30°, 45°, 60°, and 75°.
2. A point is located on the stress singularity line OA on the slanted side surface. Eigenanalysis is performed for a model with slant angles of 30°, 45°, 60°, and 75°.
3. A point is located on the stress singularity line OB on the flat side. At this location, eigenanalysis can be performed only for a slant angle of 90°.

The properties of the materials used in the eigenanalysis are shown in Table 1.

The mesh division developed on the $\theta - \phi$ plane is shown in Fig. 2 (Pageau et al. (1996)). This mesh is $\theta \times \phi = 15° \times 15°$ mesh for the model with a slant angle of 75° at the vertex. The interface of the joint is located at $\theta = 90°$. For different slant angles, the mesh division was modified based on the angle of slanted side surface.

2.2.2. Model for BEM analysis

Fig. 3 represents a model for the 3D bonded structure used in the BEM analysis. The dimensions of the model are 20 $\times$ 20 $\times$ 20 mm. Considering the symmetry of the bonded structure, the model is a one-quarter section of the bonded structure, as indicated by the bold line. The displacement in the z-direction on the bottom of the model is fixed. A tensile stress of 1 MPa is applied to the top of the model in the z-direction. The total numbers of elements and nodes are 2166 and 6500, respectively.

3. Results and discussion

3.1. Eigenanalysis

The order of a stress singularity, λ, at the vertex and at a point along the singularity line for slant angles of 30°, 45°, 60°, 75°, and 90° was calculated. The values of λ for various Young's moduli in material 2, i.e., E_2, combined with the material properties of silicon in material 1, E_1, are shown in Fig. 4. The order of the stress

Table 1
Material properties used in the analysis.

	Young's modulus E (GPa)	Poisson's ratio ν
Silicon	166	0.26
Various material	$2 \times 10^{-2} \sim 29.72580 \times 10^5$	0.38

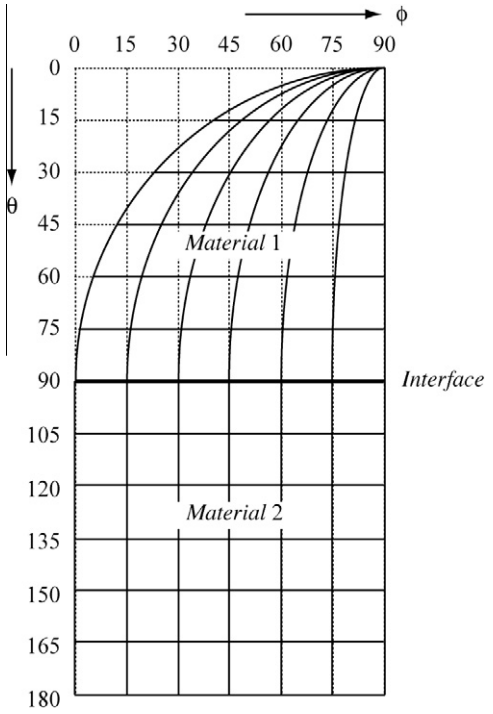

Fig. 2. Mesh division with a slanted side surface.

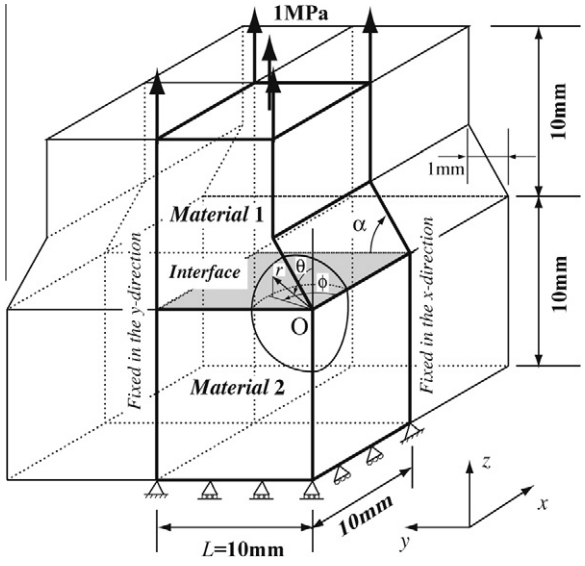

Fig. 3. Model for BEM analysis.

singularity was found to be influenced by the slant angle, α. In the range of $E_2/E_1 < 1$, a stress singularity exists for all slant angles. The stress singularity exists for the range of $E_2/E_1 > 1$ at slant angles of 60° and 75°, but does not exist for slant angles of 30° and 45°. At a point on the stress singularity line on the slanted side surface, the stress singularity exists for all slant angles in the range of $E_2/E_1 < 1$ and exists only for the slant angle of 75° in the range of $E_2/E_1 > 1$. The stress singularity exists for all different material combinations at the point on the singularity line on the flat side surface, as shown in Fig. 4(c). The subscripts of λ in Fig. 4 refer to the vertex at point O and lines OA and OB that are defined in Fig. 1.

The stress distribution at the vertex in a stress singular field will be expressed for the spherical coordinate system, as follows:

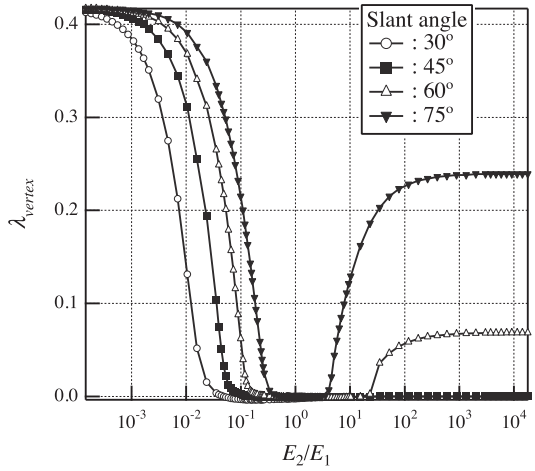

(*a*) At the vertex

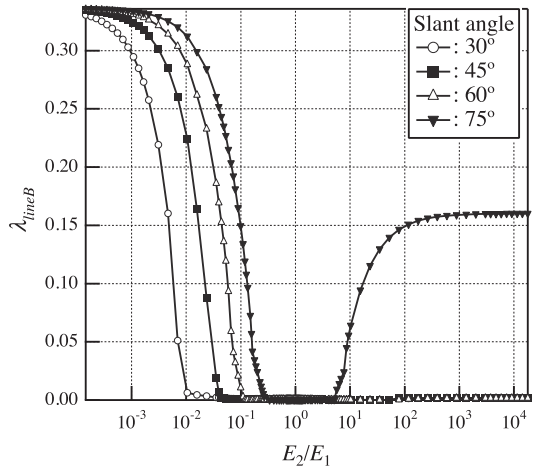

(*b*) At the slanted side surface (Line OA)

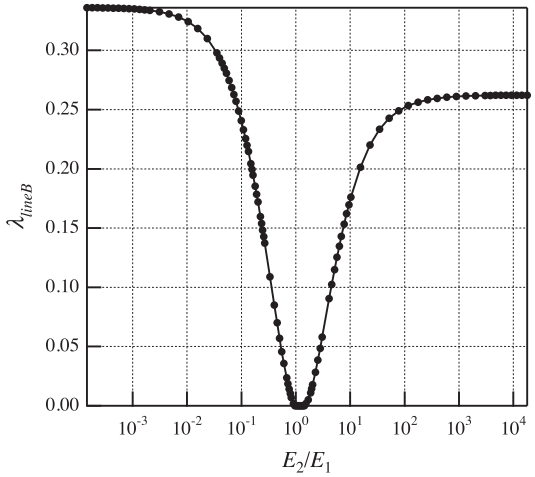

(*c*) At the flat side surface (Line OB)

Fig. 4. Relationship between the order of stress singularity and the Young's modulus ratio, E_2/E_1.

$$\sigma_{ij}^{s}(r,\theta,\phi) = \widetilde{K}_{1ij}^{s} f_{1ij}(\theta,\phi) r^{-\lambda_{vertex}} + \widetilde{K}_{2ij}^{s} f_{2ij}(\theta,\phi), \tag{3}$$

where r is a distance from the vertex, $\widetilde{K}_{kij}^{s}$ ($k = 1, 2$) is the intensity of singularity, and $f_{kij}(\theta,\phi)$ ($k = 1, 2$) are the angular functions for the stress component, σ_{ij}. Here, superscript s in σ_{ij} and K_{kij} refers to the spherical coordinate system.

3.2. Angular functions

In this section, the characteristics of angular functions is investigated using a silicon-resin joint as an example. Material properties used in the analysis are shown in Table 2. The results of eigenanalysis for several slant angles are shown in Table 3. Fig. 5 represents the distribution of angular functions for $\lambda_{vertex} = 0.255$ with respect to angle ϕ on the interface in the joint with a slant angle of 45°. The angular functions, $f_{1\theta\theta}$, $f_{1r\theta}$, and $f_{1\phi\theta}$, correspond to the stress components, $\sigma_{\theta\theta}$, $\sigma_{r\theta}$ and $\sigma_{\phi\theta}$. In this figure, the angular functions for $f_{1\theta\theta}$ and $f_{1r\theta}$ are asymmetric due to the slanted side surface. The angular function cannot be normalized using the maximum value, because the value of the angular function increases as ϕ approaches 0 and $\pi/2$, where the stress singularity lines exist. Hence, $f_{1\theta\theta}$ and $f_{1\phi\theta}$ may have a singularity at $\phi = 0$ and $\pi/2$. The value of f_{1ij} is normalized using the value at $\phi = 44.25°$, because the extrema of the angular functions of $f_{1\theta\theta}$ and $f_{1r\theta}$ exists at this point.

Angular functions, f_{1ij}, at the vertex may be characterized by the distance from the stress singularity line (see Fig. 6). Here, a cylindrical coordinate system is taken along the stress singularity line. Now, a point A on the line is taken as shown in Fig. 6(b). The stress distribution in cross section APQ can be expressed using a power law of the order of singularity for the stress singularity line as follows:

$$\sigma^c_{1ij}(r_{AP}, \Theta) = H_{1ij} r_{AP}^{-\lambda_{lineA}} g_{1ij}(\Theta), \tag{4}$$

where $g_{1ij}(\Theta)$ are the angular functions for the order of singularity, λ_{lineA}, σ^c_{1ij} is the stress for the cylindrical coordinate system, suffixes i and j take R and Θ, where Θ is the angle between AP and AQ, and r_{AP} is the distance from point A to point P on the sphere. Here, the sphere that is used in the formulation of the eigenequation is considered. First, r_{AP} is expressed as in the angles θ and ϕ. The stress is then normalized by dividing Eq. (4) by $H_{1ij}\hat{r}_{AP}^{-\lambda_{lineA}}$, where $\hat{r}_{AP}(= r_0\sqrt{1-\sin^2\theta_m\cos^2\phi_m} = r_0\ a_m)$ represents the distance at which the extremum of stress occurs. Here, θ_m and ϕ_m represent the angles yielding the extremum stress. The normalized stresses in the cylindrical coordinate system are represented by h^c_{ij}, which are transformed into the stresses in the spherical coordinate system

Table 2
Material properties used in the analysis: *silicon-resin joint*.

		Young's modulus E (GPa)	Poisson's ratio ν
Material 1	Silicon	166	0.26
Material 2	Resin	2.74	0.38

Table 3
Order of stress singularity in a silicon-resin joint for several slanted side surfaces.

Slant angle	The order of singularity		
	Vertex λ_{vertex}	Slant side λ_{lineA}	Flat side λ_{lineB}
45	0.255	0.164	0.318
60	0.343	0.262	0.318
75	0.378	0.299	0.318

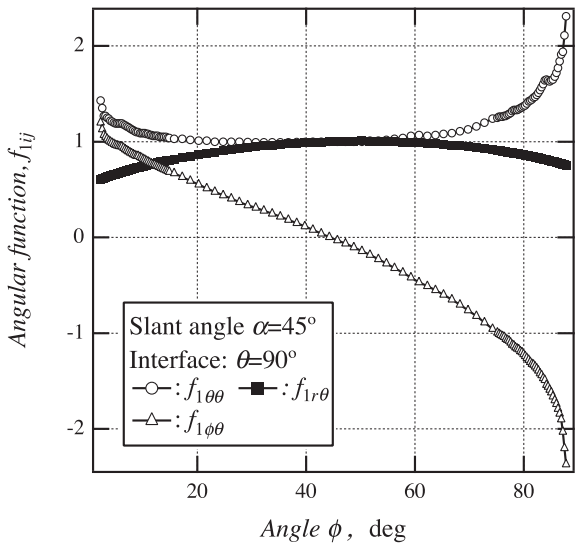

Fig. 5. Angular functions for $\lambda_{vertex} = 0.255$ at the vertex on the interface at slant angle $\alpha = 45°$.

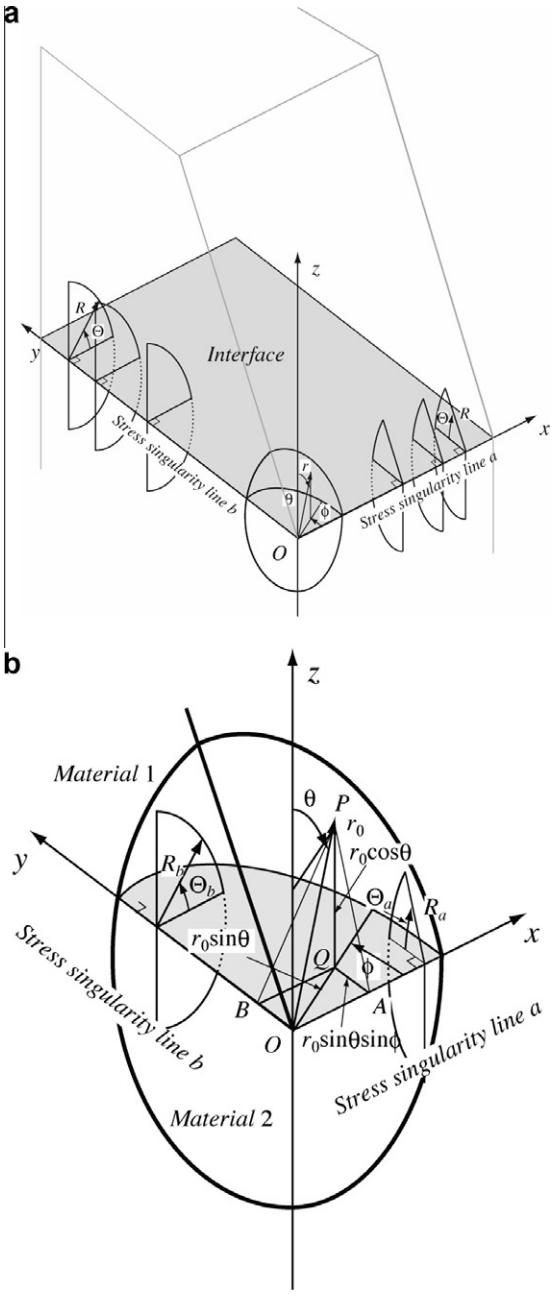

Fig. 6. (a) Spherical and cylindrical coordinate systems at the vertex and the stress singularity line. (b) Relationship between distance r_{AP} and angle ϕ.

using the formulation given in the Appendix. Here, the angular functions in the spherical coordinate system, i.e., $f_{1\theta\theta}$, $f_{1r\theta}$, and $f_{1\phi\theta}$, on the interface (at $\theta=\pi/2$, $\Theta=0$) are expressed in terms of the normalized stresses, h^c_{ij}, in the cylindrical coordinate system (A6) as follows:

$$\begin{aligned} f_{1\theta\theta} &= h^c_{\Theta\Theta}, \\ f_{1r\theta} &= -h^c_{R\Theta}\sin\phi - h^c_{x\Theta}\cos\phi, \\ f_{1\phi\theta} &= -h^c_{R\Theta}\cos\phi + h^c_{x\Theta}\sin\phi, \end{aligned} \tag{5}$$

where $h^c_{x\Theta}$, $h^c_{R\Theta}$ and $h^c_{\Theta\Theta}$ represent the normalized stress for $\sigma_{x\Theta}$, $\sigma_{R\Theta}$ and $\sigma_{\Theta\Theta}$, respectively. Substituting Eq. (4) into Eq. (5) yields:

$$f^A_{1\theta\theta}(\phi) = a_m^{\lambda_{lineA}}(\sin\phi)^{-\lambda_{lineA}} g^A_{1\Theta\Theta}(0)/g^A_{1\Theta\Theta}(\Theta_m) = L^A_{1\theta\theta}(\sin\phi)^{-\lambda_{lineA}},$$

$$\begin{aligned} f^A_{1r\theta}(\phi) &= -a_m^{\lambda_{lineA}}(\sin\phi)^{1-\lambda_{lineA}} g^A_{1R\Theta}(0)/g^A_{1R\Theta}(\Theta_m) \\ &\quad - a_m^{\lambda_{lineA}}(\sin\phi)^{-\lambda_{lineA}}\cos\phi g^A_{1x\Theta}(0)/g^A_{1x\Theta}(\Theta_m) \\ &= L^A_{1r\theta}(\sin\phi)^{-\lambda_{lineA}}\cos\phi + L^A_{2r\theta}(\sin\phi)^{1-\lambda_{lineA}}, \end{aligned} \tag{6}$$

$$\begin{aligned} f^A_{1\phi\theta}(\phi) &= -a_m^{\lambda_{lineA}}(\sin\phi)^{-\lambda_{lineA}}\cos\phi\, g^A_{1R\Theta}(0)/g^A_{1R\Theta}(\Theta_m) \\ &\quad + a_m^{\lambda_{lineA}}(\sin\phi)^{1-\lambda_{lineA}}\, g^A_{1x\Theta}(0)/g^A_{1x\Theta}(\Theta_m) \\ &= L^A_{1\phi\theta}(\sin\phi)^{-\lambda_{lineA}}\cos\phi + L^A_{2\phi\theta}(\sin\phi)^{1-\lambda_{lineA}}, \end{aligned}$$

where superscript A in f^A_{1ij} indicates that the angular function corresponding to the stress singularity line OA. Coefficients, $\pm a_m^{\lambda_{lineA}} g^A_{1ij}(0)/g^A_{1ij}(\Theta_m)$, $(i,j = R,\Theta,x)$, in the right side are replaced as L^A_{kls}, $(k = 1,2;\ l,s = r,\theta,\phi)$ Eq. (6) reveals that $f^A_{1\theta\theta}, f^A_{1r\theta}$, and $f^A_{1\phi\theta}$ have a singularity for the stresses $h_{\theta\theta}$, $h_{\phi\theta}$, and $h_{r\theta}$ on the singularity line as ϕ approaches zero. The angular functions for the side of the stress singularity line, OB, can be expressed in a similar manner to those for the stress singularity line, OA.

Adding a constant term to the expressions and substituting the angular functions f^s_{1ij} into Eq. (3) yields:

$$\begin{aligned} \sigma^s_{\theta\theta}(r,\pi/2,\phi) &= K^s_{1\theta\theta}\left[\begin{Bmatrix} L^A_{1\theta\theta}(\sin\phi)^{-\lambda_{lineA}} \\ L^B_{1\theta\theta}(\cos\phi)^{-\lambda_{lineB}} \end{Bmatrix} + \begin{Bmatrix} L^{*A}_{2\theta\theta} \\ L^{*B}_{2\theta\theta} \end{Bmatrix}\right] r^{-\lambda_{vertex}} \\ &\quad + K^s_{2\theta\theta} f_{2\theta\theta}(\pi/2,\phi), \end{aligned} \tag{7}$$

$$\begin{aligned} \sigma^s_{r\theta}(r,\pi/2,\phi) &= K^s_{1r\theta}\left[\begin{Bmatrix} L^A_{1r\theta}(\sin\phi)^{-\lambda_{lineA}}\cos\phi + L^A_{2r\theta}(\sin\phi)^{1-\lambda_{lineA}} \\ L^B_{1r\theta}(\cos\phi)^{-\lambda_{lineB}}\sin\phi + L^B_{2r\theta}(\cos\phi)^{1-\lambda_{lineB}} \end{Bmatrix}\right. \\ &\quad \left. + \begin{Bmatrix} L^A_{3r\theta}\sin\phi + L^A_{4r\theta}\cos\phi \\ L^B_{3r\theta}\cos\phi + L^B_{4r\theta}\sin\phi \end{Bmatrix}\right] r^{-\lambda_{vertex}} + K^s_{2r\theta} f_{2r\theta}(\pi/2,\phi) \end{aligned} \tag{8}$$

$$\begin{aligned} \sigma^s_{\phi\theta}(r,\pi/2,\phi) &= K^s_{1\phi\theta}\left[\begin{Bmatrix} L^A_{1\phi\theta}(\sin\phi)^{-\lambda_{lineA}}\cos\phi + L^A_{2\phi\theta}(\sin\phi)^{1-\lambda_{lineA}} \\ L^B_{1\phi\theta}(\cos\phi)^{-\lambda_{lineB}}\sin\phi + L^B_{2\phi\theta}(\cos\phi)^{1-\lambda_{lineB}} \end{Bmatrix}\right. \\ &\quad \left. + \begin{Bmatrix} L^A_{3\phi\theta}\sin\phi + L^A_{4\phi\theta}\cos\phi \\ L^B_{3\phi\theta}\cos\phi + L^B_{4\phi\theta}\sin\phi \end{Bmatrix}\right] r^{-\lambda_{vertex}} + K^s_{2\phi\theta} f_{2\phi\theta}(\pi/2,\phi) \end{aligned} \tag{9}$$

In Eqs. (7)–(9), the upper right-hand expression is the expression for the stress singularity line, OA, and the lower right-hand expression is the expression for the stress singularity line, OB.

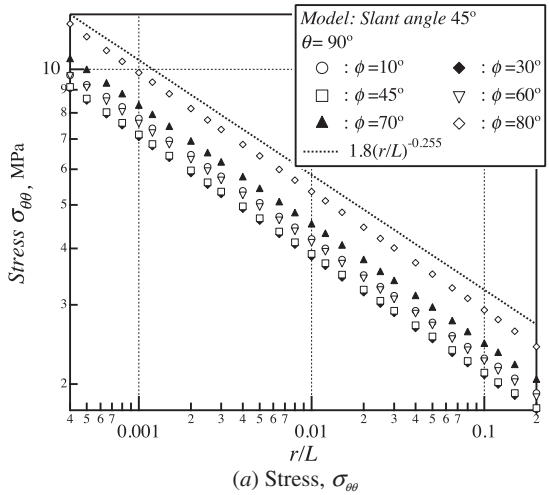

(a) Stress, $\sigma_{\theta\theta}$

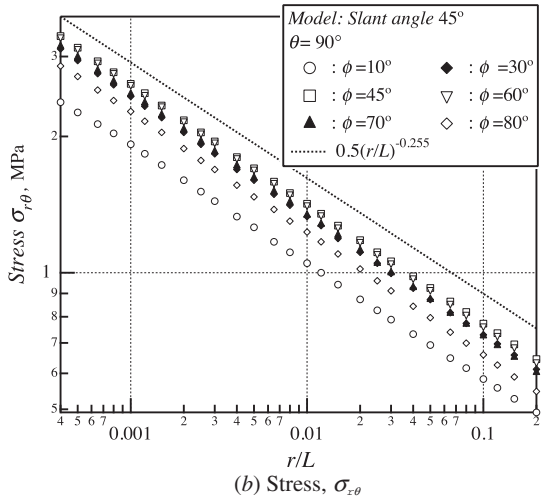

(b) Stress, $\sigma_{r\theta}$

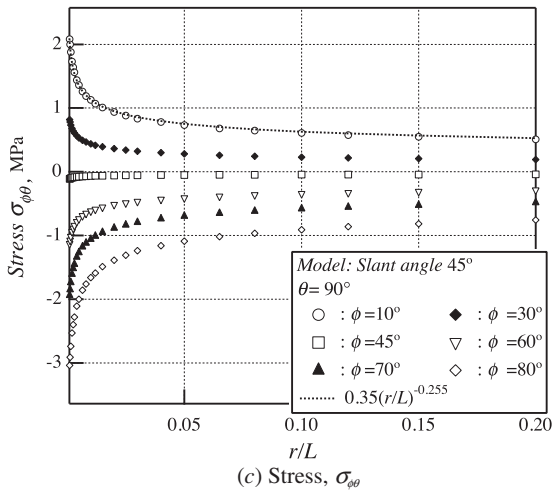

(c) Stress, $\sigma_{\phi\theta}$

Fig. 7. Distributions of stress with respect to distance r/L on the interface for a slant angle of 45°.

3.3. Boundary element analysis

The stress distributions in the stress singular field for the bonded structures with side surfaces for several slant angles are obtained using the boundary element method, and the intensities of singularity in the r- and the ϕ-directions will be determined from the stress distributions. The results for silicon-resin joint shown in Table 2 are mainly demonstrated. Finally, the intensities of stress singularity at a 3D vertex for a various material combinations are determined.

3.3.1. Stress analysis in the r-direction

Figs. 7 and 8 demonstrate the distributions of stress components, $\sigma_{\theta\theta}$, $\sigma_{r\theta}$, and $\sigma_{\phi\theta}$ with respect to r/L (L = 10 mm) on the interface in the joints for slant angles of 45° and 75°. The plots for stresses $\sigma_{\theta\theta}$ and $\sigma_{r\theta}$ are parallel in both logarithmic graphs. The dashed lines in Figs. 7 and 8 indicate the line for $C(r/L)^{-\lambda vextex}$, where C is a constant from 0.35 to 1.8, λ_{vertex} represents the order of singularity at the vertex obtained from the eigenanalysis. The slope of the stress distributions is in good agreement with the results of the eigenanalysis shown in Table 3. This means that the power law singularity governs the stress field near the vertex.

K_{kij} f_{kij} $(\pi/2, \phi\ )$ (k = 1, 2) in Eq. (3) are determined from the stress distributions on the interface. Here, $K_{1ij} = L^{\lambda vertex}\widetilde{K}^{s}_{1ij}$ and

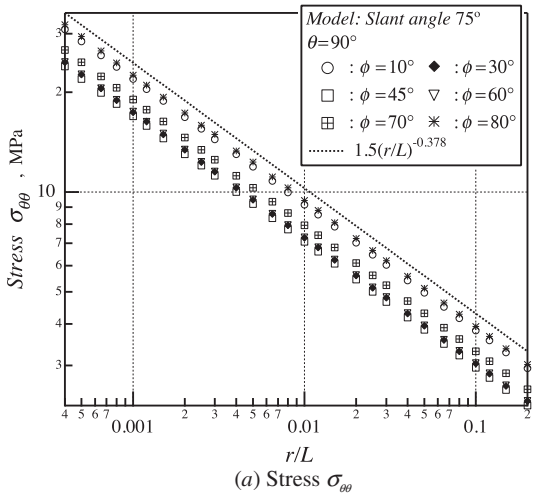

(a) Stress $\sigma_{\theta\theta}$

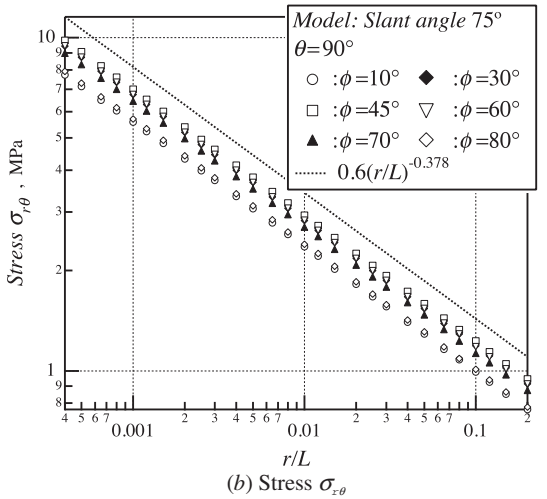

(b) Stress $\sigma_{r\theta}$

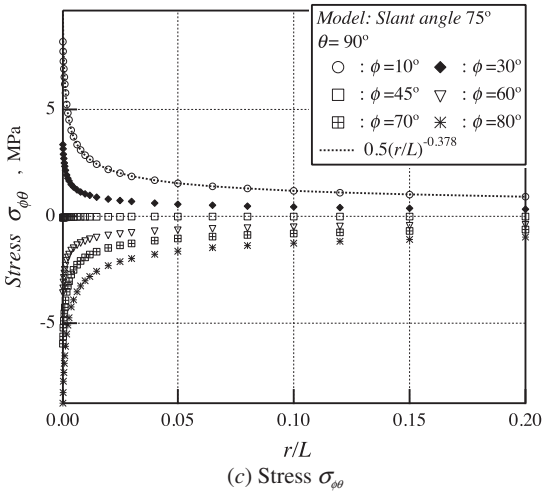

(c) Stress $\sigma_{\phi\theta}$

Fig. 8. Distributions of stress with respect to distance r/L on the interface for a slant angle of 75°.

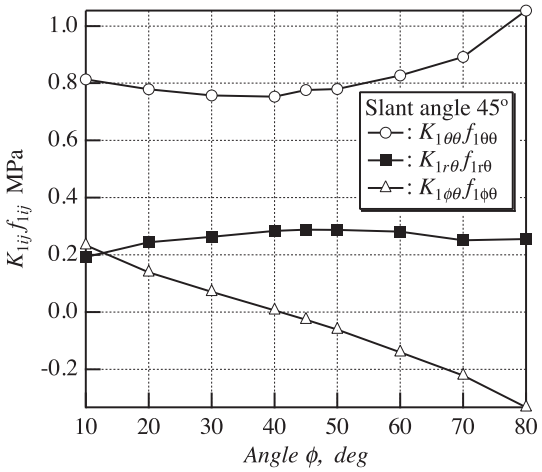

(a) Slant angle: 45°

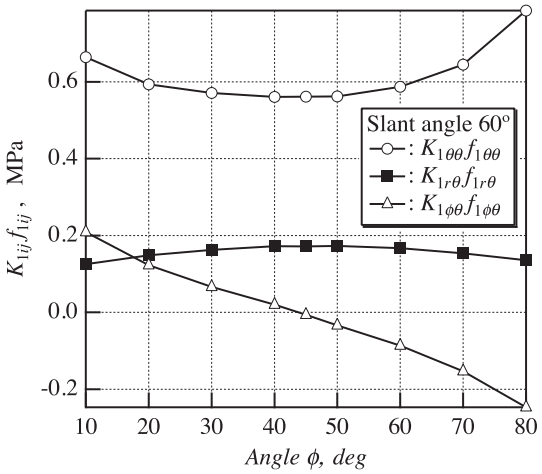

(b) Slant angle: 60°

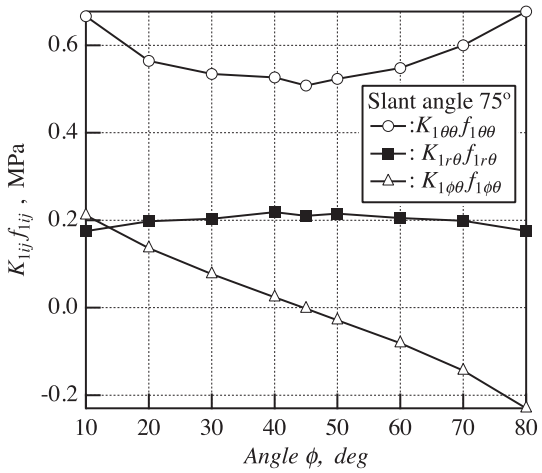

(c) Slant angle: 75°

Fig. 9. Variation of $K_{1ij}\,f_{1ij}\,(\pi/2, \phi\ )$ with respect to angle ϕ.

$K_{2ij} = \widetilde{K}^{s}_{2ij}$. Fig. 9 shows the variation of $K_{1ij} f_{1ij}(\pi/2, \phi)$ with respect to the angle ϕ in joints of slant angles 45°, 60°, and 75°. It is found that $K_{1ij} f_{1ij}(\pi/2, \phi)$ varies with angle ϕ in a manner similar to the angular functions shown in Fig. 5. The values of $K_{1ij} f_{1ij}$ are shown in Table 4, and K_{1ij} at the extremum of $K_{1ij} f_{1ij}$ is shown in Table 5. Here, f_{1ij} is set to be 1 at the extremum point.

3.3.2. Stress analysis in the ϕ-direction

Fig. 10(a)–(c) show the distributions of normalized stresses $\sigma^*_{\theta\theta}, \sigma^*_{r\theta}$, and $\sigma^*_{\phi\theta}$ at r=0.01 mm with respect to angle ϕ for different slant angles. In these figures, stresses $\sigma_{\theta\theta}$ and $\sigma_{r\theta}$ are normalized by the values at $\phi = \pi/4$, and stress $\sigma_{\phi\theta}$ is normalized by the value at 80°. These distributions are found to be similar to the angular function f_{ij} with respect to angle ϕ, as shown in Fig. 5. Fig. 11 shows both logarithmic plots of $\sigma^*_{\theta\theta}$ and angle ϕ for $\alpha = 45°$. The stresses near $\phi = 0$ and $\pi/2$ are found to have singularities with respect to angle ϕ. The slope near $\phi = 0$ is approximately equal to the order of stress singularity on the stress singularity line on the slanted side surface, OA, and that near $\phi = \pi/2$ is in approximately agreement with the order of stress singularity on the stress singularity line on flat side surface, OB. Hence, these stress distributions are approximated using Eq. (6), and the coefficients L^A_{kij} and L^B_{kij} are determined using a least squares method. The values of the coefficient are shown in Table 6.

3.3.3. 3D intensity of stress singularity

The intensity of stress singularity at the vertex is defined as $K^{3D}_{1ij} = K_{1ij} L^B_{1ij}$ from Eqs. (7)–(9). Here, the value of L^B_{1ij} on side B is chosen for estimating the intensity of singularity, because it is larger than that of L^A_{1ij} on side A. It is found that this definition of K^{3D}_{1ij} includes the influence of the vertex in the r-direction and the singularity lines on the stress singularity in the ϕ -direction. The values of K^{3D}_{1ij} for silicon-resin joints are shown in Table 7. The analysis revealed that $K^{3D}_{1\theta\theta}$ for $\sigma_{\theta\theta}$ is the largest, and this stress component is related to delamination of the interface.

Next, the intensities of the stress singularity for various Young's moduli of material 2 are investigated. Here, Young's modulus of material 1 is fixed as that of resin, and Young's modulus of material 2 is varied as shown in Table 8. The 3D intensities of the singularity K^{3D}_{1ij} with respect to E_2/E_1 are shown in Fig. 12. The value of $K^{3D}_{1\theta\theta}$ was larger that of $K^{3D}_{1r\theta}$ and $K^{3D}_{1\theta\theta}$. The intensities of the singularity depend on the existence of stress singularity, i.e., the order of the singularity at the vertex is $0 < \lambda_{vertex} < 1$, and the intensities vary with E_2/E_1 in a manner similar to the order of te singularity, as shown in Fig. 13.

Table 4
Intensity of stress singularity $K_{1ij} f_{1ij}$ for angle ϕ.

ϕ (°)	$K_{1\theta\theta} f_{1\theta\theta}$ (MPa) (at ϕ = 45°)	$K_{1r\theta} f_{1r\theta}$ (MPa) (at ϕ = 45°)	$K_{1\phi\theta}\phi_{1\phi\theta}$ (MPa) (at ϕ = 77.5°)
10	0.813	0.192	0.234
20	0.779	0.244	0.139
30	0.757	0.263	0.071
40	0.753	0.284	0.006
45	0.776	0.288	−0.027
50	0.785	0.287	−0.061
60	0.827	0.281	−0.141
70	0.892	0.251	−0.222
77.5	0.992	0.217	−0.293
80	1.0535	0.204	−0.3327

Table 5
Value of K_{1ij} at the extremum of $K_{1ij} f_{1ij}$.

Slant angle (°)	$K_{1\theta\theta}$ (MPa) ($f_{1\theta\theta}$ = 1 at ϕ = 45°)	$K_{1r\theta}$ (MPa) ($f_{1r\theta}$ = 1 at ϕ = 45°)	$K_{1\phi\theta}$ (MPa)
45	0.776	0.288	−0.293 ($f_{1\phi\theta}$ = 1 at ϕ = 77.5°)
60	0.561	0.222	−0.216 ($f_{1\phi\theta}$ = 1 at ϕ = 77.5°)
75	0.508	0.210	−0.230 ($f_{1\phi\theta}$ = 1 at ϕ = 80°)

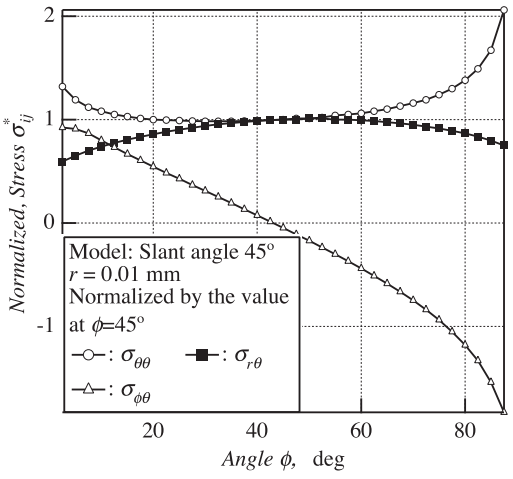

(*a*) Slant angle: 45°

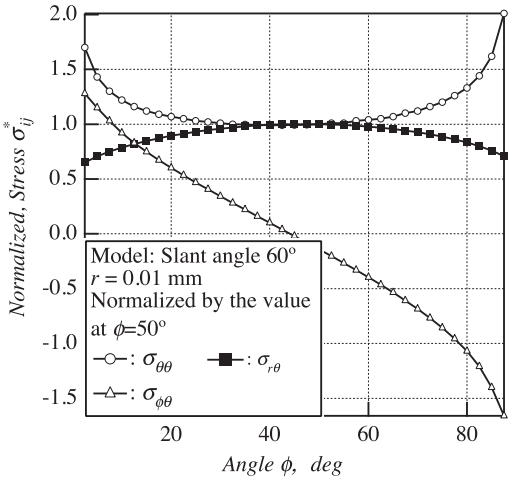

(*b*) Slant angle: 60°

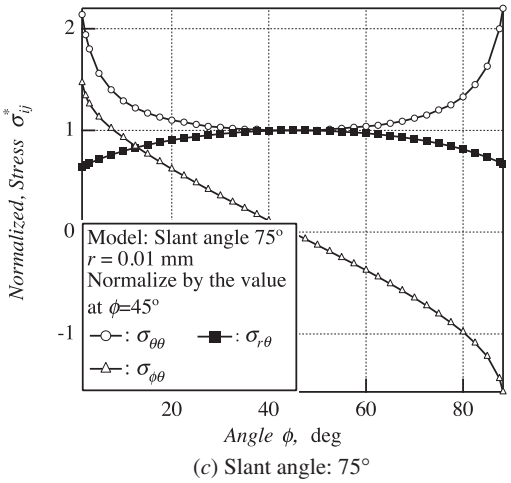

(*c*) Slant angle: 75°

Fig. 10. Normalized stress distribution on the interface at r = 0.01 mm with respect to angle ϕ.

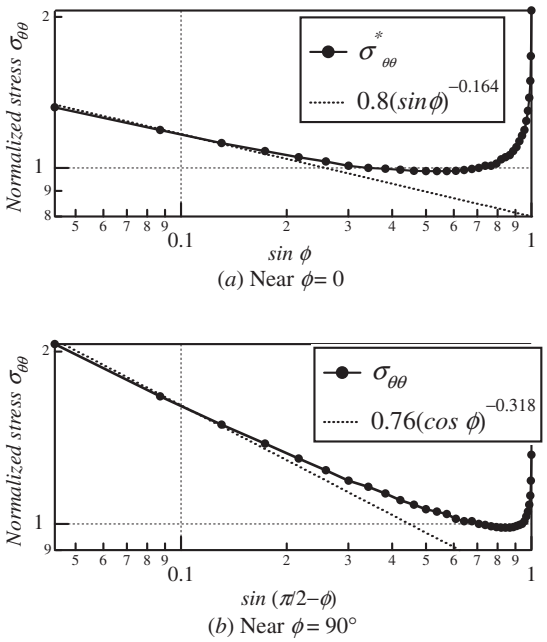

Fig. 11. Logarithmic plots of normalized stress, $\sigma_{\theta\theta}$, with respect to ϕ.

Table 6
Coefficients of angular function for the BEM results.

f^{BEM}_{qq}		f^{BEM}_{rq}		$f^{BEM}_{\phi q}$	
(a) Slant angle: 45°					
L^{A}_{1qq}	0.609	L^{A}_{1rq}	−0.069	$L^{A}_{1\phi q}$	0.414
L^{B}_{1qq}	0.675	L^{B}_{1rq}	−0.011	$L^{B}_{1\phi q}$	0.897
$L^{A,B}_{2qq}$	−0.407	L^{A}_{2rq}	1.234	$L^{A}_{2\phi q}$	0.442
		L^{B}_{2rq}	0.667	$L^{B}_{2\phi q}$	−0.046
		L^{A}_{3rq}	−0.528		
		L^{B}_{3rq}	−0.024		
(b) Slant angle: 60°					
L^{A}_{1qq}	0.6578	L^{A}_{1rq}	−0.017024	$L^{A}_{1\phi q}$	0.4222
L^{B}_{1qq}	0.6629	L^{B}_{1rq}	−0.00765	$L^{B}_{1\phi q}$	0.5243
$L^{A,B}_{2qq}$	−0.4764	L^{A}_{2rq}	1.0439	$L^{A}_{2\phi q}$	0.3946
		L^{B}_{2rq}	0.8388	$L^{B}_{2\phi q}$	0.2992
		L^{A}_{3rq}	−0.4034		
		L^{B}_{3rq}	−0.2355		
(c) Slant angle: 75°					
L^{A}_{1qq}	0.6559	L^{A}_{1rq}	−0.0168	$L^{A}_{1\phi q}$	0.3206
L^{B}_{1qq}	0.6620	L^{B}_{1rq}	−0.0232	$L^{B}_{1\phi q}$	0.3618
$L^{A,B}_{2qq}$	−0.4755	L^{A}_{2rq}	0.7046	$L^{A}_{2\phi q}$	0.5395
–	–	L^{B}_{2rq}	0.5529	$L^{B}_{2\phi q}$	0.5005
–	–	L^{A}_{3rq}	−0.0208	–	–
–	–	L^{B}_{3rq}	0.0818	–	–

Table 7
Intensity of 3D singularity.

Slant angle (°)	$K^{3D}_{\theta\theta}$(MPa)	$K^{3D}_{r\theta}$(MPa)	$K^{3D}_{\phi\theta}$(MPa)
45	0.524	−0.003	−0.263
60	0.372	−0.0016	−0.113
75	0.336	−0.0049	−0.083

When the order of the stress singularity is reduced, stress does not increase as the distance from the vertex of the interface decreases. Even if the angle of one side surface is varied, the stress distribution will vary largely. This indicates that the reliability of

Table 8
Material properties used in the analysis for calculating the three-dimensional intensity of stress singularity.

	Young's modulus E (GPa)	Poisson's ratio ν
Resin	2.74	0.38
Various materials	0.002 ~ 250	0.26

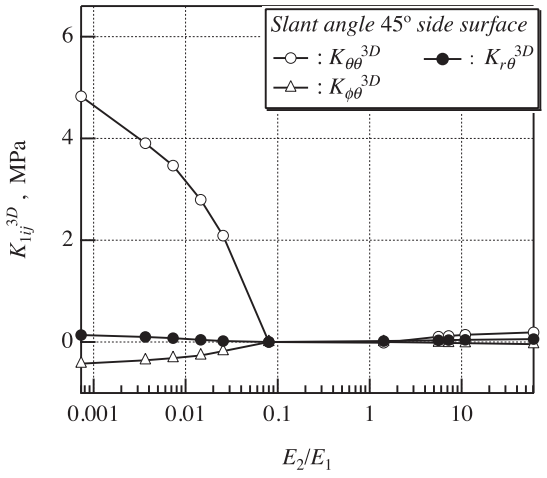

(a) Slant angle: 45°

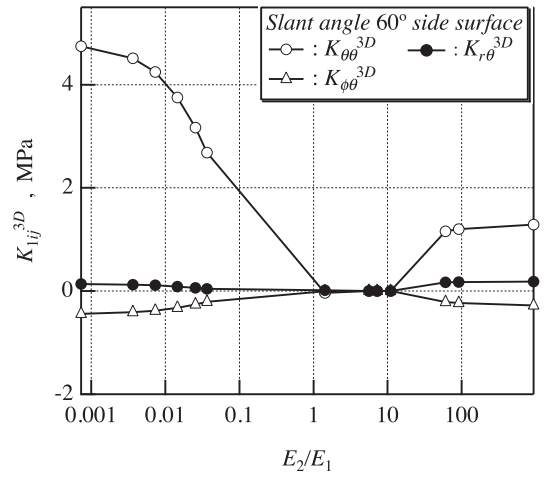

(b) Slant angle: 60°

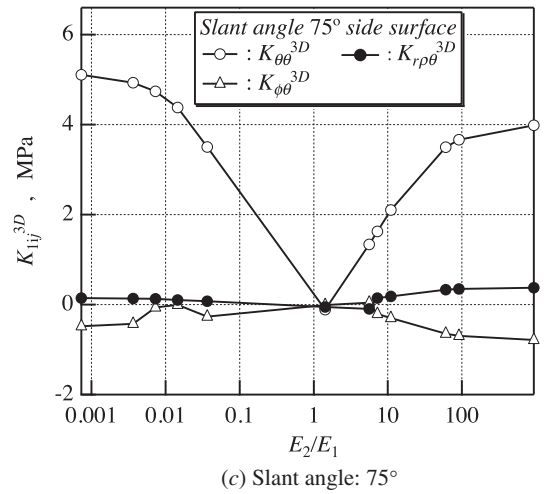

(c) Slant angle: 75°

Fig. 12. Relationship between K^{3D}_{1ij} and the ratio E_2/E_1.

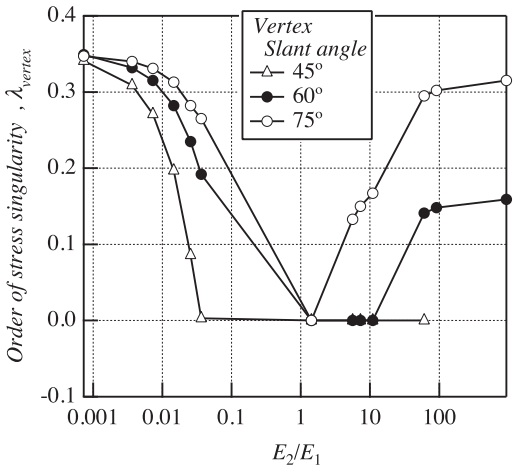

(*a*) At the vertex

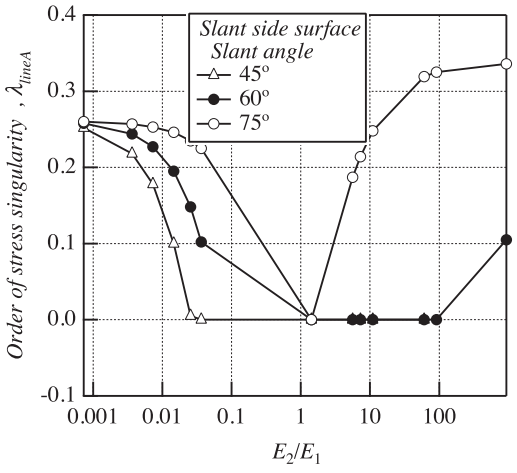

(*b*) At the slanted side surface (Line OA)

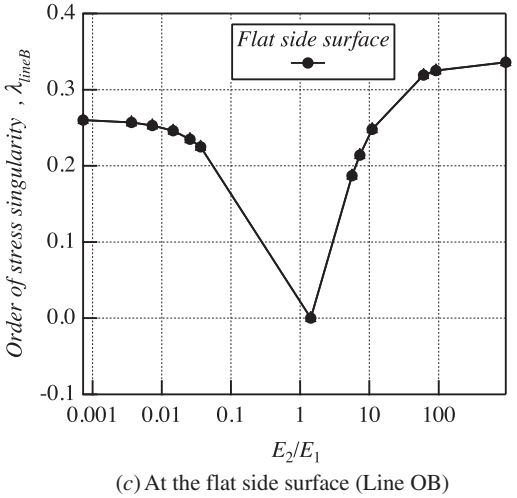

(*c*) At the flat side surface (Line OB)

Fig. 13. Relationship between the order of stress singularity and the ratio E_2/E_1.

joints might be improved by changing the angle of one side surface surrounding the vertex of the interface.

4. Conclusion

In the present paper, the intensity and order of a stress singularity, which characterize a stress singular field at a vertex in 3D joints with slanted side surfaces, were investigated using eigenanalysis and boundary element analysis. In eigenanalysis, the orders of the stress singularity at the vertex and at a point on the stress singularity lines were determined, and angular functions were obtained.

The order of the stress singularity was influenced by the slanted side surface, which could reduce the region of the stress singularity and extended the non-singularity region with respect to E_2/E_1. The slanted side surface also influences the angular function, the value of which on the slanted side surface ($\phi = 0$) is lower than that on the flat side surface ($\phi = 90°$).

The results of the BEM analysis revealed that stress near the flat side surface is larger than that near the slanted side surface. The 3D intensities of the singularity were defined and determined using the larger value in L^A_{1ij} and L^B_{1ij}. The value of $K^{3D}_{1\theta\theta}$ was larger than the values of $K^{3D}_{1r\theta}$ and $K^{3D}_{1\phi\theta}$ on the flat side in the condition for the analysis.

Acknowledgements

The present study is supported in part by a grant-in-aid for Scientific Research (21360051B) from Japan Government. The authors would like to express our gratitude to Mr. Y. Saito and Dr. T. Kurahashi for their contributions in preparing the numerical data and for their helpful discussions.

Appendix A

The formulation for coordinate transformation from a cylindrical coordinate system to a spherical coordinate system is shown below. Here, the stress components for the order of singularity in the spherical and cylindrical coordinate systems are expressed as follows:

$$\mathbf{s}^s = \begin{bmatrix} \sigma_{rr} & \sigma_{r\phi} & \sigma_{r\theta} \\ \sigma_{r\phi} & \sigma_{\phi\phi} & \sigma_{\phi\theta} \\ \sigma_{r\theta} & \sigma_{\phi\theta} & \sigma_{\theta\theta} \end{bmatrix}, \quad \mathbf{s}^c = \begin{bmatrix} \sigma_{xx} & \sigma_{xR} & \sigma_{x\Theta} \\ \sigma_{xR} & \sigma_{RR} & \sigma_{R\Theta} \\ \sigma_{x\Theta} & \sigma_{R\Theta} & \sigma_{\Theta\Theta} \end{bmatrix}, \tag{A1}$$

where the suffixes *s* and *c* indicate the spherical and cylindrical coordinate systems, respectively. Here, it is supposed that an axis of the cylindrical coordinate is directed along the *x*-axis in Fig. 6. Then, the transform matrices from the spherical coordinate system to the Cartesian coordinate system and from the cylindrical coordinate system to the Cartesian coordinate system are as follows:

$${}_s\mathbf{\Omega} = \begin{bmatrix} \cos\phi\sin\theta & \sin\phi\sin\theta & \cos\theta \\ -\sin\phi & \cos\phi & 0 \\ \cos\phi\cos\theta & \sin\phi\cos\theta & -\sin\theta \end{bmatrix}, \tag{A2}$$

$${}_c\Omega = \begin{bmatrix} 1 & 0 & 0 \\ 0 & \cos\Theta & \sin\Theta \\ 0 & -\sin\Theta & \cos\Theta \end{bmatrix}. \tag{A3}$$

The stress components in the Cartesian coordinate system can be expressed as

$$\mathbf{s}^{rec} = {}_s\mathbf{\Omega}^{-1}\mathbf{s}^s\left({}_s\mathbf{\Omega}^T\right)^{-1} = {}_c\mathbf{\Omega}^{-1}\mathbf{s}^c\left({}_c\mathbf{\Omega}^T\right)^{-1}. \tag{A4}$$

The stress components in the spherical coordinate system are expressed in terms of the stress components in the cylindrical coordinate system as follows:

$$\mathbf{s}^s = {}_s\mathbf{\Omega}\cdot\mathbf{s}^{rec}\cdot{}_s\mathbf{\Omega}^T = {}_s\mathbf{\Omega}\cdot{}_c\mathbf{\Omega}^{-1}\mathbf{s}^c\left({}_c\mathbf{\Omega}^T\right)^{-1}\cdot{}_s\mathbf{\Omega}^T. \tag{A5}$$

The stresses on the interface are obtained by substituting $\Theta = 0$ and $\theta = \pi/2$:

$$
\begin{aligned}
\sigma^s_{\theta\theta} &= \sigma^c_{\Theta\Theta},\\
\sigma^s_{r\theta} &= -\sigma^c_{x\Theta}\cos\phi - \sigma^c_{R\Theta}\sin\phi,\\
\sigma^s_{\phi\theta} &= -\sigma^c_{R\Theta}\cos\phi + \sigma^c_{x\Theta}\sin\phi,\\
\sigma^s_{rr} &= \sigma^c_{xx}\cos^2\phi + \sigma^c_{RR}\sin^2\phi + \sigma^c_{xR}\sin 2\phi,\\
\sigma^s_{r\phi} &= \sigma^c_{xR}\cos^2\phi + \left(\sigma^c_{RR} - \sigma^c_{xx}\right)\cos\phi\sin\phi - \sigma^c_{xR}\sin^2\phi,\\
\sigma^s_{\phi\phi} &= \sigma^c_{RR}\cos^2\phi + \sigma^c_{xx}\sin^2\phi - \sigma^c_{xR}\sin 2\phi.
\end{aligned}
\tag{A6}
$$

References

Apel, T., Leguillon, D., Pester, C., Yosibash, Z., 2008. Edge singularities and structure of the 3-D Williams expansion. C.R. Mecanique 336, 629–635.

Bogy, D.B., 1971. Two edge-bonded elastic wedges of different materials and wedge angles under surface tractions. J. Appl. Mech. Trans. ASME 38 (2), 377–386.

Bogy, D.B., Wang, K.C., 1971. Stress singularities at interface corners in bonded dissimilar isotropic elastic materials. Int. J. Solids Struct. 7 (4), 993–1005.

Constabel, M., Dauge, M., Lafranche, Y., 2001. Fast semi-analytic computation of elastic edge singularities. Comput. Meth. Appl. Mech. Eng. 190, 2111–2134.

Cook, T.S., Erdogan, F., 1972. Stress in bonded materials with a crack terminating at a material interface. Int. J. Eng. Sci. 10, 677–697.

Dempsey, J.P., Sinclair, G.B., 1979. On the stress singularities in the plane elasticity of the composite wedge. J. Elasticity 9 (4), 373–391.

Dimitrov, A., Andra, H., Schnack, E., 2001. Efficient computation of order and mode of corner singularities in 3D-elasticity. Int. J. Numer. Meth. Eng. 52, 805–827.

Dimitrov, A., Andra, H., Schnack, E., 2002. Singularities near three-dimensional corners in composite laminates. Int. J. Fract. 115, 361–375.

Fenner, D.N., 1976. Stress singularities in composite materials with an arbitrarily oriented crack meeting an interface. Int. J. Fract. 12 (5), 705–721.

Hein, V.L., Erdogan, F., 1971. Stress singularity in two materials wedge. Int. J. Fract. Mech. 7 (3), 317–330.

Inoue, T., Koguchi, H., Yada, T., 1995. Stress singularity near apex in three-phase bonded structure (effect of elastic property of intermediate material on order of stress singularity). JSME Int. J. A - Mech. Mater. Eng. 38 (2), 163–170.

Koguchi, H., 1996. Stress singularity analysis in three-dimensional bonded structure. Int. J. Solids Struct. 34, 461–480.

Koguchi, H., 2006. Stress singularity analysis in three-dimensional bonded structure. Trans. JSME A 72 (724), 2058–2065.

Koguchi, H., Hino, T., Kikuchi, Y., Yada, T., 1994. Residual stress analysis of joints of ceramics and metals. Exp. Mech. 34 (2), 116–124.

Koguchi, H., Muramoto, T., 2000. The order of stress singularity near the vertex in three-dimensional joints. Int. J. Solids Struct. 37, 4737–4762.

Lee, Y., Im, S., 2003. On the computation of the near-tip stress intensities for three-dimensional wedges via two-state *M*-integral. J. Mech. Phys. Solids 51, 825–850.

Omer, N., Yosibash, Z., 2008. Edge singularities in 3-D elastic anisotropic and multi-material domains. Comput. Meth. Appl. Mech. Eng. 197, 959–978.

Pageau, S.S., Biggers Jr., S.B., 1995. Finite element evaluation of free-edge singular stress fields in anisotropic materials. Int. J. Numer. Meth. Eng. 38, 2225–2239.

Pageau, S.S., Joseph, P.F., Biggers Jr., S.B., 1995. Finite element analysis of anisotropic materials with singular inplane stress fields. Int. J. Solids Struct. 32, 571–591.

Pageau, S.S., Joseph, P.F., Biggers Jr., S.B., 1996. A finite element approach to three-dimensional singular stress states in anisotropic multi-material wedges and junctions. Int. J. Solids Struct. 33, 33–47.

Prukvilailert, M., Koguchi, H., 2005. Stress singularity analysis around the singular point on the stress singularity line in three-dimensional joints. Int. J. Solids Struct. 42, 3059–3074.

Theocaris, P.S., 1974. The singularity at a multi-wedge corner of a composite plate. Int. J. Eng. Sci. 12, 107–120.

Yamada, Y., Okumura, H., 1981. Analysis of local stress in composite materials by the 3-D finite element. In: Kawata, K., Akasaka, T., (Eds.), Proceedings of the Japan–USA Conference, pp. 55–64.

Yang, Y.Y., Munz, D., 1995. Stress intensity factor and stress distribution in a joint with an interface corner under thermal and mechanical loading. Comput. Struct. 57 (3), 467–476.

Yosibash, Z., Omer, N., Dauge, M., 2008. Edge stress intensity functions in 3-D anisotropic composites. Compos. Sci. Technol. 68, 1216–1224.